Experimental protection against evolution of states in a subspace via a super-Zeno scheme on an NMR quantum information processor

Harpreet Singh,[*] Arvind ,[†] and Kavita Dorai[‡]
Department of Physical Sciences, Indian Institute of Science Education & Research (IISER) Mohali, Sector 81 SAS Nagar, Manauli PO 140306 Punjab India
(Received 9 September 2014; published 24 November 2014)

We experimentally demonstrate the freezing of evolution of quantum states in one- and two-dimensional subspaces of two qubits, on an NMR quantum information processor. State evolution was frozen and leakage of the state from its subspace to an orthogonal subspace was successfully prevented using super-Zeno sequences [Phys. Rev. Lett. **96**, 100405 (2006)], comprising a set of radio frequency (rf) pulses punctuated by pre-selected time intervals. We demonstrate the efficacy of the scheme by preserving different types of states, including separable and maximally entangled states in one- and two-dimensional subspaces of two qubits. The change in the experimental density matrices was tracked by carrying out full state tomography at several time points. We use the fidelity measure for the one-dimensional case and the leakage (fraction) into the orthogonal subspace for the two-dimensional case, as qualitative indicators to estimate the resemblance of the density matrix at a later time to the initially prepared density matrix. For the case of entangled states, we additionally compute an entanglement parameter to indicate the presence of entanglement in the state at different times. We experimentally demonstrate that the super-Zeno scheme is able to successfully confine state evolution to the one- or two-dimensional subspace being protected.

DOI: 10.1103/PhysRevA.90.052329 PACS number(s): 03.67.Pp, 03.65.Xp

I. INTRODUCTION

Using frequent measurements to project a quantum system back to its initial state and hence slow down its time evolution is a phenomenon known as the quantum Zeno effect [1–3]. If the measurements project the system back into a finite-dimensional subspace that includes the initial state, the state evolution remains confined within this subspace and the subspace can be protected against leakage of population using a quantum Zeno strategy [4,5]. An operator version of this phenomenon has also been suggested recently [6,7]. Zeno-like schemes have been used for error prevention [8], and to enhance the entanglement of a state and bring it to a Bell state, even after entanglement sudden death [9,10]. It has been shown that under certain assumptions, the Zeno effect can be realized with weak measurements and can protect an unknown encoded state against environment effects [11]. An interesting quantum Zeno-type strategy for state preservation, achieved using a sequence of nonperiodic short duration pulses, has been termed the super-Zeno scheme [12]. The super-Zeno scheme does not assume any Hamiltonian symmetry, does not involve projective quantum measurements, and achieves a significant betterment of the leakage probability as compared to standard Zeno-based preservation schemes. Similar schemes involving dynamical decoupling have been devised to suppress qubit pure dephasing and relaxation [13,14]. Another scheme to preserve entanglement in a two-qubit spin-coupled system has been constructed, which unlike the super-Zeno scheme, is based on a sequence of operations performed periodically on the system in a given time interval [15].

There are several experimental implementations of the quantum Zeno phenomenon, including suppressing unitary evolution driven by external fields between the two states of a trapped ion [16], in atomic systems [17] and suppressing failure events in a linear optics quantum computing scheme [18]. Decoherence control in a superconducting qubit system has been proposed using the quantum Zeno effect [19]. Unlike the super-Zeno and dynamical decoupling schemes that are based on unitary pulses, the quantum Zeno effect achieves suppression of state evolution using projective measurements. The quantum Zeno effect was first demonstrated in NMR by a set of symmetric π pulses [20], wherein pulsed magnetic field gradients and controlled-NOT gates were used to mimic projective measurements. The entanglement preservation of a Bell state in a two-spin system in the presence of anisotropy was demonstrated using a preservation procedure involving free evolution and unitary operations [21]. An NMR scheme to preserve a separable state was constructed using the super-Zeno scheme and the state preservation was found to be more efficient as compared to the standard Zeno scheme [22]. The quantum Zeno effect was used to stabilize superpositions of states of NMR qubits against dephasing, using an ancilla to perform the measurement [23]. Entanglement preservation based on a dynamic quantum Zeno effect was demonstrated using NMR wherein frequent measurements were implemented through entangling the target and measuring qubits [24].

This work focuses on two applications of the super-Zeno scheme: (i) preservation of a state by freezing state evolution (one-dimensional subspace protection) and (ii) subspace preservation by preventing leakage of population to an orthogonal subspace (two-dimensional subspace protection). Both kinds of protection schemes are experimentally demonstrated on separable as well as on maximally entangled two-qubit states. One-dimensional subspace protection is demonstrated on the separable $|11\rangle$ state and on the maximally entangled $\frac{1}{\sqrt{2}}(|01\rangle - |10\rangle)$ (singlet) state. Two-dimensional subspace preservation is demonstrated by choosing the $\{|01\rangle, |10\rangle\}$ subspace in the four-dimensional Hilbert space of two qubits, and

[*]harpreetsingh@iisermohali.ac.in
[†]arvind@iisermohali.ac.in
[‡]kavita@iisermohali.ac.in

implementing the super-Zeno subspace preservation protocol on three different states, namely $|01\rangle$, $|10\rangle$ and $\frac{1}{\sqrt{2}}(|01\rangle - |10\rangle)$ (singlet) states. Complete state tomography is utilized to compute experimental density matrices at several time points. State fidelities at these time points were computed to evaluate how closely the states resemble the initially prepared states, with and without super-Zeno protection. The success of the super-Zeno scheme in protecting states in the two-dimensional subspace spanned by $\{|01\rangle,|10\rangle\}$ is evaluated by computing a leakage parameter, which computes leakage to the orthogonal subspace spanned by $\{|00\rangle,|11\rangle\}$. For entangled states, an additional entanglement parameter is constructed to quantify the residual entanglement in the state over time. State fidelities, the leakage parameter, and the entanglement parameter are plotted as a function of time, to quantify the performance of the super-Zeno scheme.

The material in this paper is organized as follows: Sec. II gives a concise description of the theoretical super-Zeno scheme; in Sec. III and the subsections therein we describe the main experimental results, namely freezing the evolution of a separable and an entangled state and the prevention of leakage of population from a subspace, both schemes being implemented on a two-qubit NMR information processor. Section IV contains some concluding remarks.

II. THE SUPER-ZENO SCHEME

The super-Zeno algorithm to preserve quantum states has been developed along lines similar to bang-bang control schemes, and limits the quantum system's evolution to a desired subspace using a series of unitary kicks [12].

A finite-dimensional Hilbert space $\mathcal{H}$ can be written as a direct sum of two orthogonal subspaces $\mathcal{P}$ and $\mathcal{Q}$. The super-Zeno scheme involves a unitary kick $\mathbf{J}$, which can be constructed as

$$\mathbf{J} = \mathbf{Q} - \mathbf{P}, \tag{1}$$

where $\mathbf{P},\mathbf{Q}$ are the projection operators onto the subspaces $\mathcal{P},\mathcal{Q}$, respectively. The action of this specially crafted pulse $\mathbf{J}$ on a state $|\psi\rangle \in \mathcal{H}$ is as follows:

$$\mathbf{J}|\psi\rangle = -|\psi\rangle, \quad |\psi\rangle \in \mathcal{P}, \quad \mathbf{J}|\psi\rangle = |\psi\rangle, \quad |\psi\rangle \in \mathcal{Q}, \tag{2}$$

where $\mathcal{P}$ is the subspace being preserved.

The total super-Zeno sequence for N pulses is given by

$$W_N(t) = U(x_{N+1}t)\mathbf{J}\cdots\mathbf{J}U(x_2t)\mathbf{J}U(x_1t), \tag{3}$$

where U denotes unitary evolution under the system Hamiltonian and x_it is the time interval between the ith and $(i+1)$th pulse. The sequence $\{x_it\}$ of time intervals between pulses is optimized such that if the system starts out in the subspace $\mathcal{P}$, after measurement the probability of finding the system in the orthogonal subspace $\mathcal{Q}$ is minimized. In this work we used four inverting pulses interspersed with five inequal time intervals in each repetition of the preserving super-Zeno sequence. The optimized sequence is given by $\{x_i\} = \{\beta,1/4,1/2-2\beta,1/4,\beta\}$ with $\beta = (3-\sqrt{5})/8, i = 1\ldots5$ and t is a fixed time interval (we use the x_i as worked out in Ref. [12]).

The explicit form of the unitary kick $\mathbf{J}$ depends on the subspace that needs to be preserved, and in the following section, we implement several illustrative examples for both separable and entangled states embedded in one- and two-dimensional subspaces of two qubits.

III. EXPERIMENTAL DEMONSTRATION OF SUPER-ZENO STRATEGIES

A. NMR details

The two protons of the molecule cytosine encode the two qubits. The two-qubit molecular structure, system parameters, and pseudopure and thermal initial states are shown in Figs. 1(a)–1(c). The Hamiltonian of a two-qubit system in the rotating frame is given by

$$H = \sum_{i=1}^{2} \nu_i I_{iz} + \sum_{i<j,i=1}^{2} J_{ij} I_{iz} I_{jz}, \tag{4}$$

where ν_i are the Larmor frequencies of the spins and J_{ij} is the spin-spin coupling constant. An average longitudinal T_1 relaxation time of 7.4 s and an average transverse T_2 relaxation time of 3.25 s was experimentally measured for both the qubits. All experiments were performed at an ambient temperature of 298 K on a Bruker Avance III 600-MHz

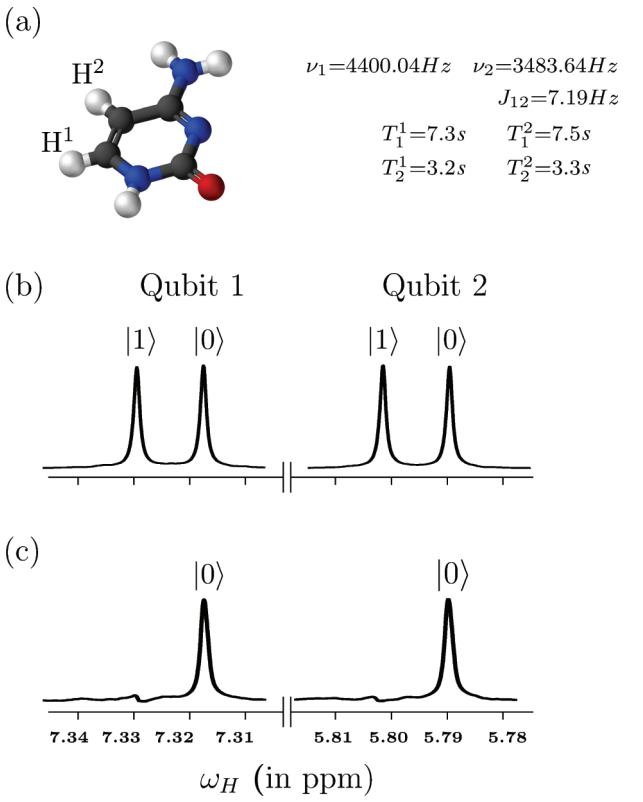

FIG. 1. (Color online) (a) Molecular structure of cytosine with the two qubits labeled as H^1 and H^2 and tabulated system parameters with chemical shifts ν_i and scalar coupling J_{12} (in Hz) and relaxation times T_1 and T_2 (in seconds). (b) NMR spectrum obtained after a $\pi/2$ readout pulse on the thermal equilibrium state. The resonance lines of each qubit are labeled by the corresponding logical states of the other qubit. (c) NMR spectrum of the pseudopure $|00\rangle$ state.

NMR spectrometer equipped with a QXI probe. The two-qubit system was initialized into the pseudopure state $|00\rangle$ using the spatial averaging technique [25], with the density operator given by

$$\rho_{00} = \frac{1-\epsilon}{4} I + \epsilon |00\rangle\langle 00|, \tag{5}$$

with a thermal polarization $\epsilon \approx 10^{-5}$ and I being a 4×4 identity operator. The experimentally created pseudopure state $|00\rangle$ was tomographed with a fidelity of 0.99. The pulse propagators for selective excitation were constructed using the GRAPE algorithm [26] to design the amplitude and phase modulated RF profiles. Selective excitation was typically achieved with pulses of duration 1 ms. Numerically generated GRAPE pulse profiles were optimized to be robust against RF inhomogeneity and had an average fidelity of $\geqslant 0.99$. All experimental density matrices were reconstructed using a reduced tomographic protocol [27], with the set of operations given by $\{II, IX, IY, XX\}$ being sufficient to determine all 15 variables for the two-qubit system. Here I is the identity (do-nothing operation) and $X(Y)$ denotes a single spin operator that can be implemented by applying a corresponding spin selective $\pi/2$ pulse. The fidelity of an experimental density matrix was computed by measuring the projection between the theoretically expected and experimentally measured states using the Uhlmann-Jozsa fidelity measure [28,29]:

$$F = (Tr(\sqrt{\sqrt{\rho_{\text{theory}}}\rho_{\text{expt}}\sqrt{\rho_{\text{theory}}}}))^2, \tag{6}$$

where ρ_{theory} and ρ_{expt} denote the theoretical and experimental density matrices, respectively.

B. Super-Zeno for state preservation

When the subspace $\mathcal{P}$ is a one-dimensional subspace, and hence consists of a single state, the super-Zeno scheme becomes a state preservation scheme.

Product states. We begin by implementing the super-Zeno scheme on the product state $|11\rangle$ of two qubits, where the Hilbert space can be decomposed as a direct sum of the subspaces $\mathcal{P} = \{|11\rangle\}$ and $\mathcal{Q} = \{|00\rangle, |01\rangle, |10\rangle)\}$. The super-Zeno pulse $\mathbf{J}$ to protect the state $|11\rangle \in \mathcal{P}$ is given by Eq. (1):

$$\mathbf{J} = I - 2|11\rangle\langle 11|, \tag{7}$$

with the corresponding matrix form,

$$\mathbf{J} = \begin{pmatrix} 1 & 0 & 0 & 0 \\ 0 & 1 & 0 & 0 \\ 0 & 0 & 1 & 0 \\ 0 & 0 & 0 & -1 \end{pmatrix}. \tag{8}$$

The super-Zeno circuit to preserve the $|11\rangle$ state, and the corresponding NMR pulse sequence is given in Fig. 2. The controlled-phase gate (Z) in Fig. 2(a) which replicates the unitary kick $\mathbf{J}$ for preservation of the $|11\rangle$ state is implemented using a set of three sequential gates: two Hadamard gates on the second qubit sandwiching a controlled-NOT gate (CNOT_{12}), with the first qubit as the control and the second qubit as the target. The Δ_i time interval in Fig. 2(a) is given by $\Delta_i = x_i t$, with x_i as defined in Eq. (3). The five Δ_i time intervals were worked to be 0.095 ms, 0.25 ms, 0.3 ms, 0.25 ms, and 0.095 ms,

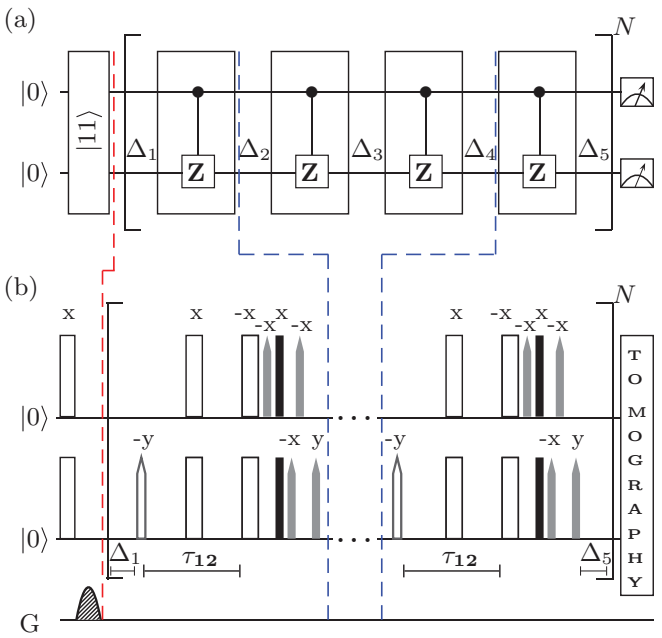

FIG. 2. (Color online) (a) Quantum circuit for preservation of the state $|11\rangle$ using the super-Zeno scheme. $\Delta_i = x_i t, (i = 1 \ldots 5)$ denote time intervals punctuating the unitary operation blocks. Each unitary operation block contains a controlled-phase gate (Z), with the first (top) qubit as the control and the second (bottom) qubit as the target. The entire scheme is repeated N times before measurement (for our experiments $N = 30$). (b) Block-wise depiction of the corresponding NMR pulse sequence. A z gradient is applied just before the super-Zeno pulses, to clean up undesired residual magnetization. The unfilled and black rectangles represent hard 180^0 and 90^0 pulses, respectively, while the unfilled and gray-shaded conical shapes represent 180^0 and 90^0 pulses (numerically optimized using GRAPE), respectively; τ_{12} is the evolution period under the J_{12} coupling. Pulses are labeled with their respective phases and unless explicitly labeled, the phase of the pulses on the second (bottom) qubit are the same as those on the first (top) qubit.

respectively, for $t = 1$ ms. One run of the super-Zeno circuit (with four inverting $\mathbf{J}$s and five Δ_i time evolution periods) takes approximately 300 ms and the entire preserving sequence $W_N(t)$ in Eq. (3) was applied 30 times. The final state of the system was reconstructed using state tomography and the real and imaginary parts of the tomographed experimental density matrices without any preservation and after applying the super-Zeno scheme, are shown in Fig. 3. The initial $|11\rangle$ state (at time $T = 0s$) was created (using the spatial averaging scheme) with a fidelity of 0.99. The tomographs (on the right in Fig. 3) clearly show that state evolution has been frozen with the super-Zeno scheme.

Entangled state preservation. We next apply the super-Zeno scheme to preserve an entangled state in our system of two qubits. We choose the singlet state $\frac{1}{\sqrt{2}}(|01\rangle - |10\rangle)$ as the entangled state to be preserved. It is well known that entanglement is an important but fragile computational resource, and constructing schemes to protect entangled states from evolving into other states is of considerable interest in quantum information processing [30].

We again write the Hilbert space as a direct sum of two subspaces: the subspace being protected and the subspace

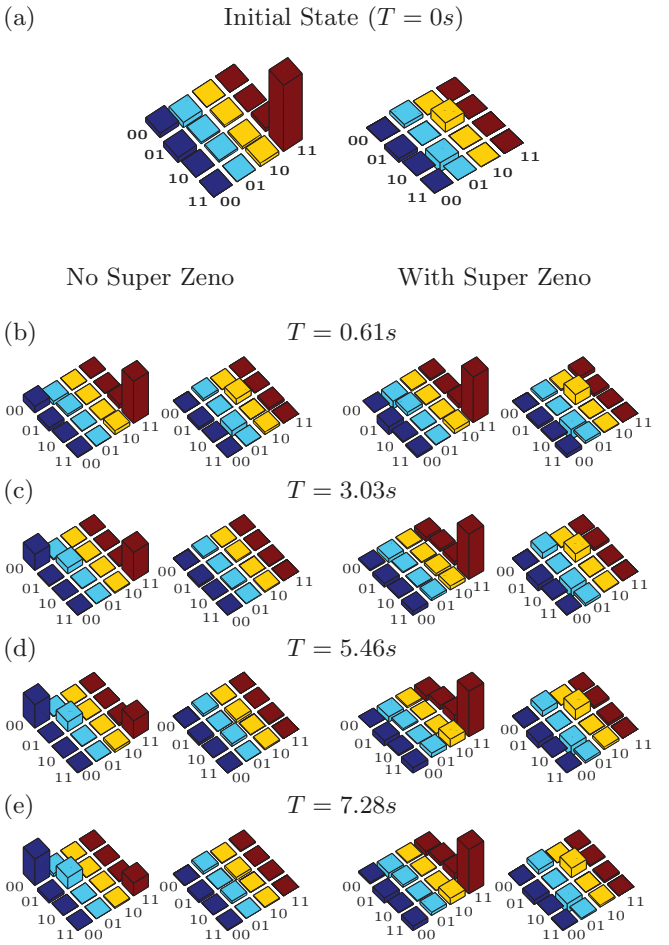

FIG. 3. (Color online) Real (left) and imaginary (right) parts of the experimental tomographs of the (a) $|11\rangle$ state, with a computed fidelity of 0.99; (b)–(e) depict the state at $T = 0.61, 3.03, 5.46, 7.28$ s, with the tomographs on the left and the right representing the state without and after applying the super-Zeno preserving scheme, respectively. The rows and columns are labeled in the computational basis ordered from $|00\rangle$ to $|11\rangle$.

orthogonal to it. In this case, the one-dimensional subspace $\mathcal{P}$ being protected is

$$\mathcal{P} = \left\{ \frac{1}{\sqrt{2}}(|01\rangle - |10\rangle) \right\}, \tag{9}$$

and the orthogonal subspace $\mathcal{Q}$ into which one would like to prevent leakage is

$$\mathcal{Q} = \left\{ \frac{1}{\sqrt{2}}(|01\rangle + |10\rangle), |00\rangle, |11\rangle \right\}. \tag{10}$$

The super-Zeno pulse to protect the singlet state as constructed using Eq. (1) is

$$\mathbf{J} = I - (|01\rangle\langle 01| + |10\rangle\langle 10| - |01\rangle\langle 10| - |10\rangle\langle 01|), \tag{11}$$

with the corresponding matrix form,

$$\mathbf{J} = \begin{pmatrix} 1 & 0 & 0 & 0 \\ 0 & 0 & 1 & 0 \\ 0 & 1 & 0 & 0 \\ 0 & 0 & 0 & 1 \end{pmatrix}. \tag{12}$$

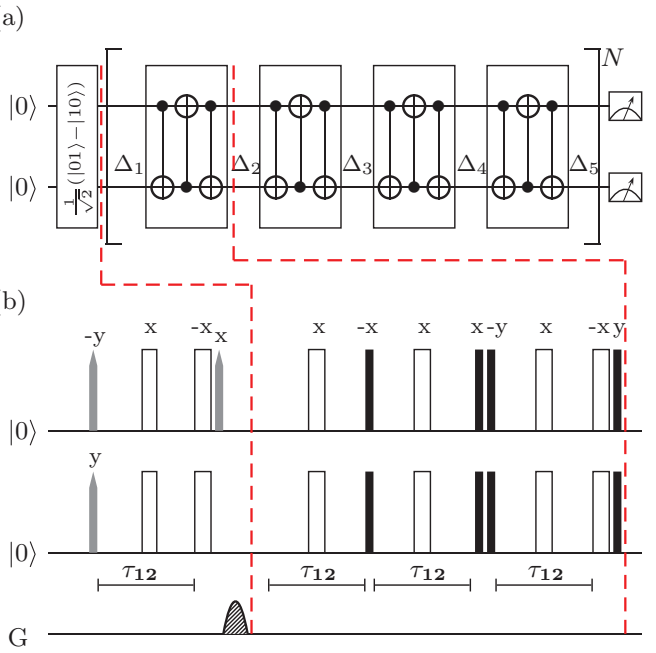

FIG. 4. (Color online) (a) Quantum circuit for preservation of the singlet state using the super-Zeno scheme. $\Delta_i, (i = 1 \ldots 5)$ denote time intervals punctuating the unitary operation blocks. The entire scheme is repeated N times before measurement (for our experiments $N = 10$). (b) NMR pulse sequence corresponding to one unitary block of the circuit in (a). A z gradient is applied just before the super-Zeno pulses to clean up undesired residual magnetization. The unfilled rectangles represent hard 180^0 pulses, the black filled rectangles representing hard 90^0 pulses, while the shaded shapes represent numerically optimized (using GRAPE) pulses and the gray-shaded shapes representing 90^0 pulses, respectively; τ_{12} is the evolution period under the J_{12} coupling. Pulses are labeled with their respective phases and unless explicitly labeled, the phase of the pulses on the second (bottom) qubit are the same as those on the first (top) qubit.

The quantum circuit and the NMR pulse sequence for preservation of the singlet state using the super-Zeno scheme are given in Fig. 4. Each **J** inverting pulse in the unitary block in the circuit is decomposed as a sequential operation of three noncommuting controlled-NOT gates: CNOT_{12}-CNOT_{21}-CNOT_{12}, where CNOT_{ij} denotes a controlled-NOT with i as the control and j as the target qubit. The five Δ_i time intervals were worked to be 0.95 ms, 2.5 ms, 3 ms, 2.5 ms, and 0.95 ms, respectively, for $t = 10$ ms. One run of the super-Zeno circuit (with four inverting **J**s and five Δ_i time evolution periods) takes approximately 847 ms and the entire super-Zeno preserving sequence $W_N(t)$ in Eq. (3), is applied 10 times. The singlet state was prepared from an initial pseudopure state $|00\rangle$ by a sequence of three gates: a nonselective NOT gate (hard π_x pulse) on both qubits, a Hadamard gate, and a CNOT_{12} gate. The singlet state thus prepared was computed to have a fidelity of 0.99. The effect of chemical shift evolution during the delays was compensated for with refocusing pulses. The final singlet state has been reconstructed using state tomography, and the real and imaginary parts of the tomographed experimental density matrices, without any preservation and after applying

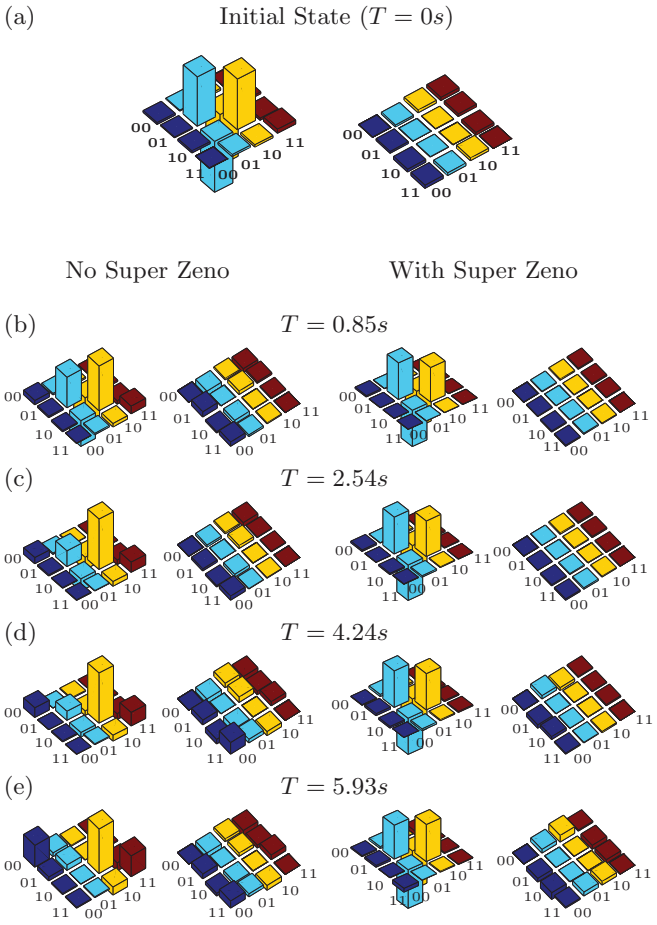

FIG. 5. (Color online) Real (left) and imaginary (right) parts of the experimental tomographs of the (a) $\frac{1}{\sqrt{2}}(|01\rangle - |10\rangle)$ (singlet) state, with a computed fidelity of 0.99; (b)–(e) depict the state at $T = 0.85, 2.54, 4.24, 5.93$ s, with the tomographs on the left and the right representing the state without and after applying the super-Zeno preserving scheme, respectively. The rows and columns are labeled in the computational basis ordered from $|00\rangle$ to $|11\rangle$.

the super-Zeno scheme, are shown in Fig. 5. As can be seen from the experimental tomographs in Fig. 5, the evolution of the singlet state is almost completely frozen by the super-Zeno sequence up to nearly 6 s, while without any preservation the state has leaked into the orthogonal subspace within 2 s.

Estimation of state fidelity. The plots of state fidelity versus time are shown in Fig. 6 for the state $|11\rangle$ and the singlet state, with and without the super-Zeno preserving sequence. The deviation density matrix is renormalized at every point and the state fidelity is estimated using the definition in Eq. (6). Renormalization is performed since our focus here is on the quantum state of the spins contributing to the signal and not in the number per se of participating spins [31]. The plots in Fig. 6 and the tomographs in Figs. 3 and 5 show that with super-Zeno protection, the state remains confined to the $|11\rangle$ (singlet) part of the density matrix, while without the protection scheme, the state leaks into the orthogonal subspace. As seen from both plots in Fig. 6, the state evolution of specific states can be arrested for quite a long time using the super-Zeno preservation scheme, while leakage probability of the state

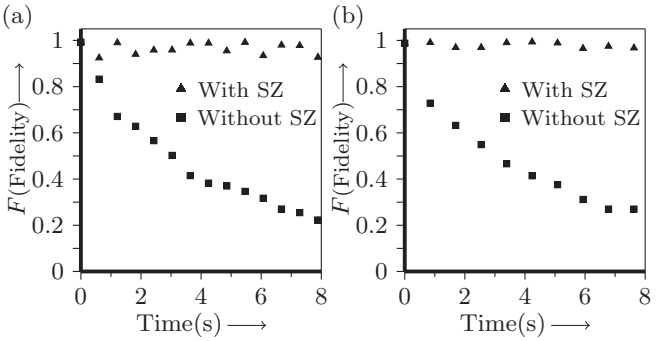

FIG. 6. Plot of fidelity versus time of (a) the $|11\rangle$ state and (b) the $\frac{1}{\sqrt{2}}(|01\rangle - |10\rangle)$ (singlet) state, without any preserving scheme and after the super-Zeno preserving sequence. The fidelity of the state with the super-Zeno preservation remains close to 1.

to other states in the orthogonal subspace spanned by $\mathcal{Q}$ is minimized. A similar renormalization procedure is adopted in the subsequent sections where we plot the leak fraction and entanglement parameters (Figs. 10 and 11).

C. Super-Zeno for subspace preservation

While in the previous subsection, the super-Zeno scheme was shown to be effective in arresting the evolution of a one-dimensional subspace (as applied to the cases of a product and an entangled state), the scheme is in fact more general. For example, if we choose a two-dimensional subspace in the state space of two qubits and protect it by the super-Zeno scheme, then any state in this subspace is expected to remain within this subspace and not leak into the orthogonal subspace. While the state can meander within this subspace, its evolution out of the subspace is frozen.

We now turn to implementing the super-Zeno scheme for subspace preservation, by constructing the **J** operator to preserve a general state embedded in a two-dimensional subspace. We choose the subspace spanned by $\mathcal{P} = \{|01\rangle, |10\rangle\}$ as the subspace to be preserved, with its orthogonal subspace now being $\mathcal{Q} = \{|00\rangle, |11\rangle\}$. It is worth noting that within the subspace being protected, we have product as well as entangled states.

The super-Zeno pulse **J** to protect a general state $|\psi\rangle \in P$ can be constructed as

$$\mathbf{J} = I - 2(|01\rangle\langle 01| - |10\rangle\langle 10|), \tag{13}$$

with the corresponding matrix form,

$$\mathbf{J} = \begin{pmatrix} 1 & 0 & 0 & 0 \\ 0 & -1 & 0 & 0 \\ 0 & 0 & -1 & 0 \\ 0 & 0 & 0 & 1 \end{pmatrix}. \tag{14}$$

The quantum circuit and corresponding NMR pulse sequence to preserve a general state in the $\{|01\rangle, |10\rangle\}$ subspace is given in Fig. 7. The unitary kick [denoted as U_{zz} in the unitary operation block in Fig. 7(a)] is implemented by tailoring the gate time to the J-coupling evolution interval of the system Hamiltonian, sandwiched by nonselective π pulses (NOT gates), to refocus undesired chemical shift evolution during the action of the gate. The five Δ_i intervals were

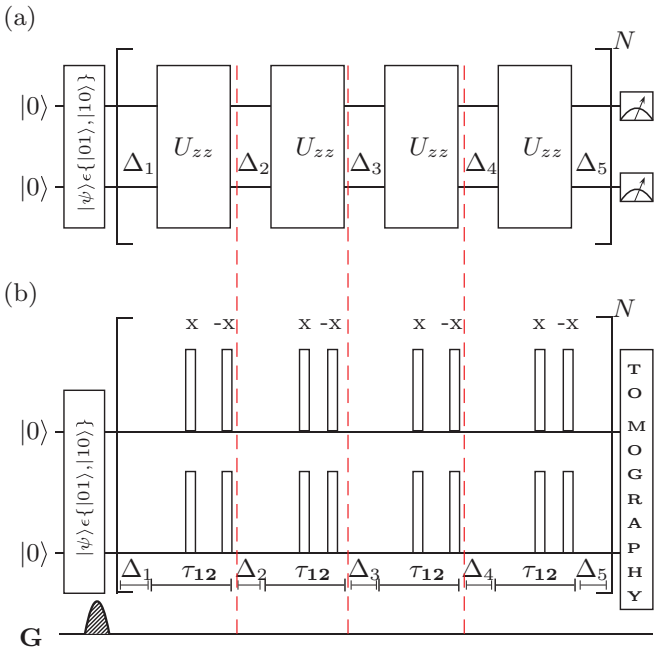

FIG. 7. (Color online) (a) Quantum circuit for preservation of the {01,10} subspace using the super-Zeno scheme. Δ_i,($i = 1...5$) denote time intervals punctuating the unitary operation blocks. The entire scheme is repeated N times before measurement (for our experiments $N = 30$). (b) NMR pulse sequence corresponding to the circuit in (a). A z gradient is applied just before the super-Zeno pulses, to clean up undesired residual magnetization. The unfilled rectangles represent hard 180^0 pulses; τ_{12} is the evolution period under the J_{12} coupling. Pulses are labeled with their respective phases.

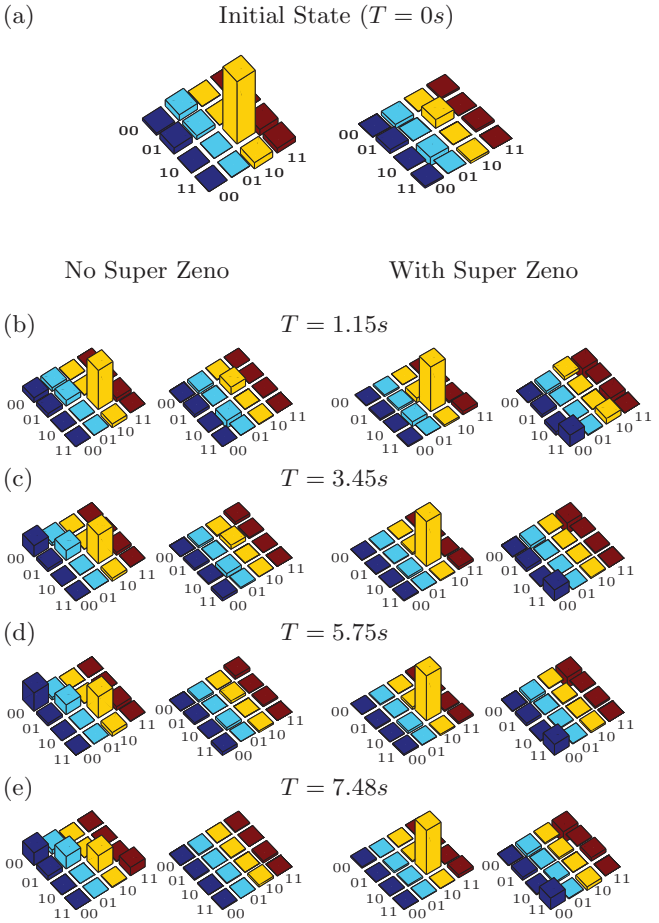

FIG. 8. (Color online) Real (left) and imaginary (right) parts of the experimental tomographs of the (a) $|10\rangle$ state in the two-dimensional subspace {01,10}, with a computed fidelity of 0.98; (b)–(e) depict the state at $T = 1.15,3.45,5.75,7.48$ s, with the tomographs on the left and the right representing the state without and after applying the super-Zeno preserving scheme, respectively. The rows and columns are labeled in the computational basis ordered from $|00\rangle$ to $|11\rangle$.

worked to be 0.95 ms, 2.5 ms, 3 ms, 2.5 ms, and 0.95 ms, respectively, for $t = 10$ ms. One run of the super-Zeno circuit (with four inverting **J**s and five Δ_i time evolution periods) takes approximately 288 ms and the entire super-Zeno preserving sequence $W_N(t)$ in Eq. (3), is applied 30 times.

Preservation of product states in the subspace. We implemented the subspace-preserving scheme on two different (separable) states $|01\rangle$ and $|10\rangle$ in the subspace $\mathcal{P}$. The efficacy of the preserving unitary is verified by tomographing the experimental density matrices at different time points and computing the state fidelity. Both the $|01\rangle$ and $|10\rangle$ states remain within the subspace $\mathcal{P}$ and do not leak out to the orthogonal subspace $\mathcal{Q} = \{|00\rangle,|11\rangle\}$.

The final $|10\rangle$ state has been reconstructed using state tomography, and the real and imaginary parts of the experimental density matrices without any preservation and after applying the super-Zeno scheme, tomographed at different time points, are shown in Fig. 8. As can be seen from the experimental tomographs, the evolution of the $|10\rangle$ state out of the subspace is almost completely frozen by the super-Zeno sequence up to nearly 7.5 s, while without any preservation the state has leaked into the orthogonal subspace within 3.5 s. The tomographs for the $|01\rangle$ state show a similar level of preservation (data not shown).

Preservation of an entangled state in the subspace. We now prepare an entangled state (the singlet state) embedded in the two-dimensional $\mathcal{P} = \{|01\rangle,|10\rangle\}$ subspace, and use the subspace-preserving scheme described in Fig. 7 to protect $\mathcal{P}$. The singlet state was reconstructed using state tomography, and the real and imaginary parts of the tomographed experimental density matrices without any preservation and after applying the super-Zeno scheme, are shown in Fig. 9. As can be seen from the experimental tomographs, the state evolution remains within the $\mathcal{P}$ subspace but the state itself does not remain maximally entangled.

Estimating leakage outside subspace. The subspace-preserving capability of the circuit given in Fig. 7 was quantified by computing a leakage parameter that defines the amount of leakage of the state to the orthogonal $\mathcal{Q} = \{|00\rangle,|11\rangle\}$ subspace. For a given density operator ρ the "leak (fraction)" δ into the subspace $\mathcal{Q}$ is defined as

$$\delta = \langle 00|\rho|00\rangle + \langle 11|\rho|11\rangle. \tag{15}$$

The leak (fraction) δ versus time is plotted in Figs. 10(a) and 10(b), for the $|10\rangle$ and the singlet state, respectively, with and without applying the super-Zeno subspace-preserving

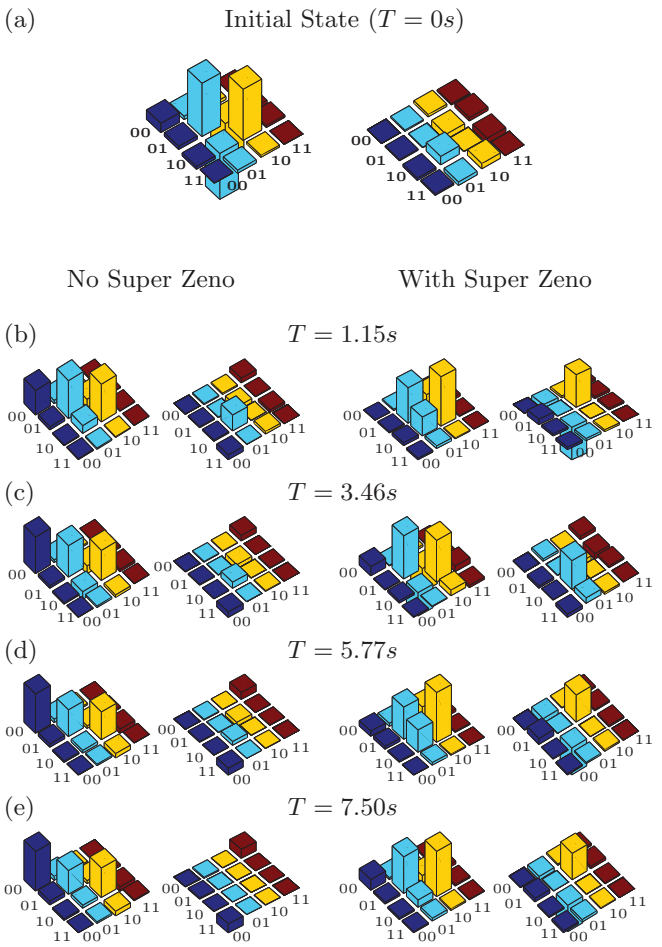

FIG. 9. (Color online) Real (left) and imaginary (right) parts of the experimental tomographs of the (a) $\frac{1}{\sqrt{2}}(|01\rangle - |10\rangle)$ (singlet) state in the two-dimensional subspace $\{01,10\}$, with a computed fidelity of 0.98; (b)–(e) depict the state at $T = 1.15,3.46,5.77,7.50$ s, with the tomographs on the left and the right representing the state without and after applying the super-Zeno preserving scheme, respectively. The rows and columns are labeled in the computational basis ordered from $|00\rangle$ to $|11\rangle$.

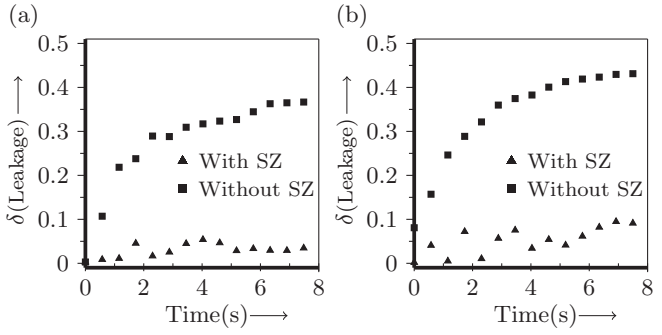

FIG. 10. Plot of leakage fraction from the $\{|01\rangle,|10\rangle\}$ subspace to its orthogonal subspace $\{|00\rangle,|11\rangle\}$ of (a) the $|10\rangle$ state and (b) the $\frac{1}{\sqrt{2}}(|01\rangle - |10\rangle)$ (singlet) state, without any preservation and after applying the super-Zeno sequence. The leakage to the orthogonal subspace is minimal (remains close to zero) after applying the super-Zeno scheme.

sequence. The leakage parameter remains close to zero for both kinds of states, proving the success and the generality of the super-Zeno scheme.

D. Preservation of entanglement

The amount of entanglement that remains in the state after a certain time is quantified by an entanglement parameter denoted by η. Since we are dealing with mixed bipartite states of two qubits, all entangled states will be negative under partial transpose (NPT). For such NPT states, a reasonable measure of entanglement is the minimum eigenvalue of the partially transposed density operator. For a given experimentally tomographed density operator ρ, we obtain ρ^{PT} by taking a partial transpose with respect to one of the qubits. The entanglement parameter η for the state ρ in terms of the smallest eigenvalue E^{ρ}_{Min} of ρ^{PT} is defined as

$$\eta = \begin{cases} -E^{\rho}_{\mathrm{Min}} & \text{if} \quad E^{\rho}_{\mathrm{Min}} < 0 \\ 0 & \text{if} \quad E^{\rho}_{\mathrm{Min}} > 0 \end{cases}. \tag{16}$$

We will use this entanglement parameter η to quantify the amount of entanglement at different times.

The maximally entangled singlet state was created and its evolution studied in two different scenarios. In the first scenario described in Sec. III B, the singlet state was protected against evolution by the application of the super-Zeno scheme. In the second scenario described in Sec. III C, a two-dimensional subspace containing the singlet state was protected using the super-Zeno scheme. For the former case, one expects that the state will remain a singlet state, while in the latter case, it can evolve within the protected two-dimensional subspace. Since in the second case, the protected subspace contains entangled as well as separable states, one does not expect preservation of entanglement to the same extent as expected in the first case, where the one-dimensional subspace defined by the singlet state itself is protected. The experimental tomographs at different times and fidelity for the case of state protection and the leakage fraction for the case of subspace protection have been discussed in detail in the previous subsections.

Here we focus our attention on the entanglement present in the state at different times. The entanglement parameter η for the evolved singlet state is plotted as a function of time and is shown in Figs. 11(a) and 11(b), after applying the state-preserving and the subspace-preserving super-Zeno sequence, respectively. In both cases, the state becomes disentangled very quickly (after approximately 2 s) if no super-Zeno preservation is performed. After applying the state-preserving super-Zeno sequence [Fig. 11(a)], the amount of entanglement in the state remains close to maximum for a long time (up to 8 s). After applying the subspace-preserving super-Zeno sequence [Fig. 11(b)], the state shows some residual entanglement over long times but it is clear that the state is no longer maximally entangled. This implies that the subspace-preserving sequence does not completely preserve the entanglement of the singlet state, as expected. However, while the singlet state becomes mixed over time, its evolution remains confined to states within the two-dimensional subspace ($\mathcal{P} = \{|01\rangle,|10\rangle\}$) being preserved as is shown in Fig. 10, where we calculate the leak (fraction).

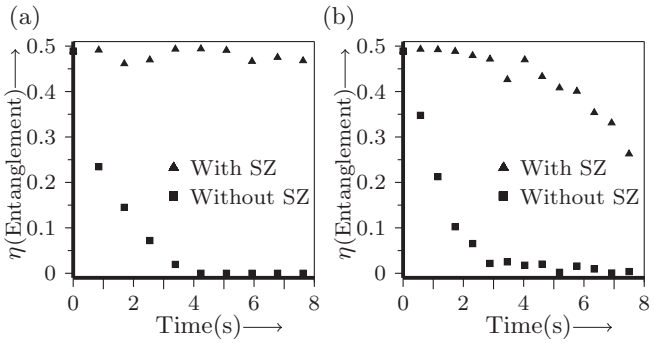

FIG. 11. Plot of entanglement parameter η with time, with and without applying the super-Zeno sequence, computed for (a) the $\frac{1}{\sqrt{2}}(|01\rangle - |10\rangle)$ (singlet) state, and (b) the same singlet state when embedded in the subspace $\{|01\rangle, |10\rangle\}$ being preserved.

IV. CONCLUDING REMARKS

In summary, we have experimentally demonstrated that the super-Zeno scheme can efficiently preserve states in one- and two-dimensional subspaces, by preventing leakage to a subspace orthogonal to the subspace being preserved. We have implemented the super-Zeno sequence on product as well as on entangled states, embedded in one- and two-dimensional subspaces of a two-qubit NMR quantum information processor.

We emphasize here that the strength of the super-Zeno protection scheme lies in its ability to preserve the state such that while the number of spins in that particular state reduces with time, the state remains the same. Without the super-Zeno protection, the number of spins in the state reduces with time and the state itself migrates towards a thermal state, reducing the fidelity. Our work adds to the arsenal of real-life attempts to protect against evolution of states in quantum computers and points the way to the possibility of developing hybrid strategies (combining the super-Zeno scheme with other schemes such as dynamical decoupling sequences) to tackle preservation of fragile computational resources such as entangled states.

ACKNOWLEDGMENTS

All experiments were performed on a Bruker Avance-III 600-MHz FT-NMR spectrometer at the NMR Research Facility at IISER Mohali. H.S. acknowledges CSIR India for financial support.

[1] C. B. Chiu, E. C. G. Sudarshan, and B. Misra, Phys. Rev. D **16**, 520 (1977).
[2] P. Facchi and M. Ligabo, J. Math. Phys. **51**, 022103 (2010).
[3] P. Facchi, G. Marmo, and S. Pascazio, J. Phys.: Conf. Ser. **196**, 012017 (2009).
[4] P. Facchi and S. Pascazio, Phys. Rev. Lett. **89**, 080401 (2002).
[5] J. Busch and A. Beige, J. Phys.: Conf. Ser. **254**, 012009 (2010).
[6] S.-C. Wang, Y. Li, X.-B. Wang, and L.-C. Kwek, Phys. Rev. Lett. **110**, 100505 (2013).
[7] Y. Li, D. A. Herrera-Marti, and L. C. Kwek, Phys. Rev. A **88**, 042321 (2013).
[8] N. Erez, Y. Aharonov, B. Reznik, and L. Vaidman, Phys. Rev. A **69**, 062315 (2004).
[9] S. Maniscalco, F. Francica, R. L. Zaffino, N. Lo Gullo, and F. Plastina, Phys. Rev. Lett. **100**, 090503 (2008).
[10] J. G. Oliveira, Jr., R. Rossi, Jr., and M. C. Nemes, Phys. Rev. A **78**, 044301 (2008).
[11] G. A. Paz-Silva, A. T. Rezakhani, J. M. Dominy, and D. A. Lidar, Phys. Rev. Lett. **108**, 080501 (2012).
[12] D. Dhar, L. K. Grover, and S. M. Roy, Phys. Rev. Lett. **96**, 100405 (2006).
[13] G. S. Uhrig, New J. Phys. **10**, 083024 (2008).
[14] W. Yang and R.-B. Liu, Phys. Rev. Lett. **101**, 180403 (2008).
[15] Y.-C. Hou, G.-F. Zhang, Y. Chen, and H. Fan, Ann. Phys. **327**, 292 (2012).
[16] W. M. Itano, D. J. Heinzen, J. J. Bollinger, and D. J. Wineland, Phys. Rev. A **41**, 2295 (1990).
[17] J. Bernu, S. Deleglise, C. Sayrin, S. Kuhr, I. Dotsenko, M. Brune, J. M. Raimond, and S. Haroche, Phys. Rev. Lett. **101**, 180402 (2008).
[18] J. D. Franson, B. C. Jacobs, and T. B. Pittman, Phys. Rev. A **70**, 062302 (2004).
[19] Q.-J. Tong, J.-H. An, L. C. Kwek, H.-G. Luo, and C. H. Oh, Phys. Rev. A **89**, 060101 (2014).
[20] L. Xiao and J. A. Jones, Phys. Lett. A **359**, 424 (2006).
[21] V. S. Manu and A. Kumar, Phys. Rev. A **89**, 052331 (2014).
[22] R. Ting-Ting, L. Jun, S. Xian-Ping, and Z. Ming-Sheng, Chin. Phys. B **18**, 4711 (2009).
[23] Y. Kondo, Y. Matsuzaki, K. Matsushima, and J. G. Filgueiras, arXiv:1406.7188.
[24] W. Zheng, D. Z. Xu, X. Peng, X. Zhou, J. Du, and C. P. Sun, Phys. Rev. A **87**, 032112 (2013).
[25] D. Cory, M. Price, and T. Havel, Physica D **120**, 82 (1998).
[26] Z. Tosner, T. Vosegaard, C. Kehlet, N. Khaneja, S. J. Glaser, and N. C. Nielsen, J. Magn. Reson. **197**, 120 (2009).
[27] G. M. Leskowitz and L. J. Mueller, Phys. Rev. A **69**, 052302 (2004).
[28] A. Uhlmann, Rep. Math. Phys. **9**, 273 (1976).
[29] R. Jozsa, J. Mod. Opt. **41**, 2315 (1994).
[30] M. A. Nielsen and I. L. Chuang, *Quantum Computation and Quantum Information* (Cambridge University Press, Cambridge, 2000).
[31] A. Gavini-Viana, A. M. Souza, D. O. Soares-Pinto, J. Teles, R. S. Sarthour, E. R. deAzevedo, T. J. Bonagamba, and I. S. Oliveira, Quant. Inf. Proc. **9**, 575 (2009).